Submitted to J. Ther. Spray Techn., Feb. 2009

HEAT TRANSFER THROUGH PLASMA SPRAYED THERMAL BARRIER COATINGS IN GAS TURBINES - A REVIEW OF RECENT WORK

*I.O. Golosnoy[§], A. Cipitria[†] & T.W. Clyne**

[§] School of Electronics and Computer Science
University of Southampton
Southampton SO17 1BJ, UK

† Department of Materials
CEIT, San Sebastián, Spain

* Department of Materials Science & Metallurgy
Cambridge University
Pembroke Street, Cambridge CB2 3QZ, UK
e-mail: twc10@cam.ac.uk

Abstract

A review is presented of how heat transfer takes place in plasma sprayed (zirconia-based) thermal barrier coatings (TBCs) during operation of gas turbines. These characteristics of TBCs are naturally of central importance to their function. Current state-of-the-art TBCs have relatively high levels of porosity (~15%) and the pore architecture (ie its morphology, connectivity and scale) has a strong influence on the heat flow. Contributions from convective, conductive and radiative heat transfer are considered, under a range of operating conditions, and the characteristics are illustrated with experimental data and modelling predictions. In fact, convective heat flow within TBCs usually makes a negligible contribution to the overall heat transfer through the coating, although what might be described as convection can be important if there are gross through-thickness defects such as segmentation cracks. Radiative heat transfer, on the other hand, can be significant within TBCs, depending on temperature and radiation scattering lengths, which in turn are sensitive to the grain structure and the pore architecture. Under most conditions of current interest, conductive heat transfer is largely predominant. However, it is not only conduction through solid ceramic that is important. Depending on the pore architecture, conduction through gas in the pores can play a significant role, particularly at the high gas pressures typically acting in gas turbines (although rarely applied in laboratory measurements of conductivity). The durability of the pore structure under service conditions is also of importance, and this review covers some recent work on how the pore architecture, and hence the conductivity, is affected by sintering phenomena. Some information is presented concerning the areas in which research and development work needs to be focussed if improvements in coating performance are to be achieved.

Keywords: Plasma Spray Coatings; Thermal Barrier Coatings, Zironia; Thermal Conductivity, Pore Connectivity; Sintering

1 Introduction

Improvement in the performance of TBCs remains a key objective for further development of power generation, marine and aeroengine gas turbines. This review is focused on Plasma Sprayed

(PS) TBCs, which are widely used in power generation and marine turbines, although most of the issues and effects described here apply equally to (zirconia) TBCs produced by Physical Vapour Deposition (PVD), which are currently used for most of the moving components in the high temperature regions of aeroengines. Gas temperatures at turbine entry can be as high as 1750 K and thermal barriers are sought giving temperature drops across them of 200 K or more. Furthermore, there is continued interest in raising turbine entry temperatures above current levels, since this is the main potential source of improvements in engine efficiency. In order to achieve this, and avoid overheating the metallic components, the thermal conductance of the coating must be low - preferably below about 1 kW m^{-2} K^{-1}, which, for a coating with a conductivity of 1 W m^{-1} K^{-1}, requires a thickness of about 1 mm. This is proving to be a major challenge, particularly since the coating must retain a low conductivity, and remain mechanically stable, when exposed to prolonged high temperatures, high heat fluxes, thermal cycling in contact with a metallic substrate (of higher thermal expansivity) and high speed impact by particulate matter. A thin coating with a low conductivity is preferable to a thicker one with a higher conductivity, since thicker coatings are more prone to spallation and also constitute a greater parasitic mass. If a coating could be devised that was thermo-mechanically stable with a thickness of about 0.5 mm, and had a conductivity under turbine operating conditions below about 0.5 W m^{-1} K^{-1}, then this would be regarded as an advance of profound significance.

The microstructure of PS TBCs comprises overlapping splats lying approximately parallel to the substrate, with interlamellar (inter-splat) pores oriented normal to the heat flux direction, through-thickness intra-splat microcracks (created during splat quenching) and globular voids. These features confer low through-thickness thermal conductivity (K~1 W m^{-1} K^{-1}) and low in-plane stiffness (E~20 GPa). The latter is beneficial in reducing the stresses that arise during thermal cycling as a consequence of the mismatch in expansivity between substrate (α ~ 11-15 10^{-6} K^{-1}) and coating (α ~ 9-11 10^{-6} K^{-1}).

Various models have been developed for simulation of heat flow through different types of composite and porous material [1, 2]. Attention is focussed here on two-component systems, in which the second component is in the form of gas-filled pores. Such systems can be modelled as incorporating randomly-distributed pores [3-6], contact resistance [7-9] or periodic structures [10, 11]. Randomly-distributed inclusions, at dilute concentrations, have been modelled, assuming them to be non-interacting [4, 5], whereas, for higher porosity levels, self-consistent [12, 13] and effective medium [3, 14] models have been developed. The latter considers an isolated inclusion to be located within a material with an effective conductivity, which differs from that of the real matrix.

Several models have been developed specifically for PS coatings and other layered systems, taken as being composed of arrays of solid lamellae, with small contact areas between them. McPherson [7] assumed two independent heat fluxes to arise in such a system, one through the contact areas and the other through the pores. He ascribed a thermal resistance to the contact regions. The thermal resistance of the lamellae [8] and oxidation of the contact areas [9] have also been incorporated into such models, with heat flow through the pores being ignored. The original 2-D shear lag analysis of Lu and Hutchinson [11], designed for cross-ply composites with matrix cracks, has since been extended to PVD TBCs by Lu et al [10], treating them as exhibiting a 2–D periodic structure of thin cracks in a uniform matrix. Golosnoy et al [15] developed a model to predict the thermal conductivity of layered structures with periodic contacts, representative of PS TBCs.

During service, TBCs are exposed to high temperatures for extended periods, leading to sintering effects. Consequently increased through-thickness thermal conductivity [16-18] has been widely

reported, and correlated with growth of the inter-splat contact area [7, 15]. It's also clear that grain growth, and associated reduction in the scattering of radiation, can contribute to increased heat transfer. Increases in coating stiffness [19-21] also occur during sintering, as a consequence of inter-splat locking and splat stiffening, leading to increased danger of spallation [18, 20, 22-26]. This is particularly problematic [27-31] when it is accelerated by the presence of impurities, such as calcia-magnesia-alumina-silica (CMAS), either from the original powder or deposited during service. This concern relates equally to both PS and PVD coatings. Recent work on the modelling of such sintering, and its effect on thermal conductivity, is included in this review.

2 Basic Heat Transfer Characteristics

2.1 Heat Flow in Porous Media

A schematic representation is shown in Fig.1 of the mechanisms by which heat transfer can occur in porous ceramic materials such as PS YSZ. Characteristics of conduction in solids, and of radiative transmission, are described in standard sources [32-34]. Conduction in gases is also well-characterised, with conductivity being dependent on the molecular mean free path, λ, which in turn is a function of temperature and pressure [35] – see Fig.1. At ambient temperature and pressure, λ has a value of about 60 nm, falling to 2 nm at 30 bar and rising to 400 nm at 2000 K. The gas conductivity within a pore is close to that of the free gas (eg $K_{air} \sim 0.025$ W m^{-1} K^{-1}), provided the dimensions of the pore are much larger than the mean free path (L>~10 λ). However, it falls below the free gas value if the pore structure is finer than this and can approach that due solely to gas molecule – wall collisions (Knudsen conduction) if L is less than λ. This would require an exceptionally fine pore structure (unless the gas pressure were low and the temperature high), but even moderately fine structures (L<~1 μm) can lead to conductivities significantly below that of the free gas. Of course, all gas conductivities are normally much lower than those of solids, which usually fall between ~1 and ~300 W m^{-1} K^{-1}.

It's worth noting that, while it's attractive for all operative heat transfer mechanisms to be incorporated into a single "conductivity" value for the coating material, this cannot be done rigorously. Even if it's assumed that convection can be ignored within TBCs (see §2.2 below), radiation is potentially significant and this contribution to the heat flux is sensitive to the absolute temperatures of the heat source and sink, rather than just the difference between them, as for conduction. Of course, it is possible to ascribe an approximate contribution to the conductivity from radiation, provided the temperatures involved are specified, but it may be preferable to model the radiative heat transfer (during operation of a gas turbine) separately from that due to conduction. Conduction through the gas in pores, and radiative heat transfer, within PS YSZ are treated in more detail below (§3.2 and §3.3).

2.2 Scale Effects, Convective Heat Transfer and Segmentation Cracks

The scale of the pore structure (and the grain size) can also affect radiative heat transfer, since radiation can be scattered by interfaces (and by grain boundaries). A fine scale structure thus tends to result in increased scattering and reduced transmission (see §3.3). Another effect of scale relates to the possibility of convection within or between pores [36-38]. It can readily be shown [2] that convective heat transfer within closed pores is only likely to be significant if they are very large (L>~10 mm). If the pressure is high (but the temperature is not), then this minimum size falls, but in general such (closed cell) convection can be neglected for most porous materials, and certainly for PS TBCs. While most porosity in TBCs is normally inter-connected, convective heat transfer

through the porosity network can also be neglected [2]. However, it should be noted that, when gross through-thickness cracks, sometimes termed "segmentation cracks" [39, 40], are present in TBCs, then flow of (high temperature) gas into them is likely to be extensive, and to effect considerable heat transfer to the substrate. This is a major drawback to having such cracks, which are sometimes seen as beneficial because they improve the mechanical stability, by relaxing residual stresses within the coating, and reducing the associated danger of spallation.

2.3 Eshelby-based Analytical Model for Porous Media

Prediction of the effective thermal conductivity is in principle straightforward for most composite systems, including porous materials (for which the voids, with or without gas content, can be treated as the added constituent or "reinforcement"). Various treatments [1, 41, 42] have been developed for prediction of the thermal conductivity of composites, as a function of the volume fraction and geometry of the "reinforcing" constituent. An example is provided by the plots shown in Fig.2, which were obtained using the Eshelby method [2, 41]. This leads to the following tensor equation for the conductivity in the presence of a volume fraction p of insulating ellipsoid-shaped voids

$$K = \left[K_{\mathrm{m}}^{-1} - p \left\{ K_{\mathrm{m}} \left[S - p(S - I) \right] - K_{\mathrm{m}} \right\}^{-1} \right]^{-1} \qquad (1)$$

where K_{m} is the matrix conductivity, S is the Eshelby tensor (dependent on ellipsoid aspect ratio s) and I is the identity tensor. The plots in Fig.2(a) are for oblate ellipsoids, with aspect ratios between unity (spheres) and zero (disk shape cracks). It can be seen from Fig.2(b) that most porous materials, including PS TBCs, exhibit conductivities below that of the Eshelby predictions for spherical inclusions. This is primarily due to inadequacies in the geometrical assumptions, since large changes in conductivity can result from the presence of cracks with high aspect ratios - see Fig.2(a). Of course, the pore architecture is in most cases more complex and convoluted than a set of isolated ellipsoids [43]. The original Eshelby method is based on a set of identical inclusions, but it is possible to create a variety of inclusions, provided they are at dilute concentrations [4, 5]. Furthermore, explicit relationships have been suggested [44] between the conductivity of a porous material in vacuum and its elastic constants. However, all methods of this type, based on an equivalent continuum representation of conductive heat flow, do have inherent limitations when applied to highly porous materials, particularly when radiative and/or convective heat transfer is possible.

It is in any event clear that a high void content can lead to a very low thermal conductivity ratio, but in practice other requirements, such as a minimum mechanical strength and erosion resistance, may also be important and in general materials that might be described as foams are not sufficiently durable for use as TBCs in the environment of a gas turbine.

2.4 Contact-based Analytical Models for plasma-sprayed TBCs

Since contacts (bridges) between splats are key features of the microstructure of PS coatings, several models based on their role have been proposed [7, 8, 15]. These incorporate appropriate combinations of a contact conductance and the conductance associated with heat flow inside splats or through gas in pores. The earliest model, that of McPherson [7], assumes small, non-interacting bridges, whereas the most recent, from Golosnoy et al [15], treats a combination of heat funnelling through regions of contact and direct conduction through surrounding regions. Contact-based models have both advantages and disadvantages in comparison with Eshelby-based models. Most of the pores in PS TBCs are interconnected and the inter-splat contacts are an integral part of the overall

architecture. Such a realistic representation of the three-dimensional geometry is important if predictions of thermal (or elastic) properties are to be linked with modelling of the microstructural evolution due to sintering. On the other hand, while it's possible to incorporate anisotropy of inter-splat crack orientation in contact models, averaging operations of this type are more complex and difficult than with generalised continuum (Eshelby method) techniques.

A comparative study of both approaches [15] has suggested that they represent different, but almost equivalent, representations of the microstructure. The major challenge for both methods is to establish reliable microstructural characterisation parameters, using whatever experimental methods are appropriate. Optical and electron (scanning and transmission) microscopy are obvious techniques, although the fine scale of the pore structure creates challenges and there are serious dangers that sectioning and polishing, and possibly other types of preparation such as fracturing, can substantially distort what is seen. In any event, such direct observation is more relevant to contact-based models than to continuum models. Other experimental techniques, such as small angle neutron scattering, appear more relevant to continuum models, but in reality their relevance and reliability remain largely unproven.

3 Heat Flow in Plasma Sprayed Zirconia

3.1 Composition and Microstructure

A wide range of base materials has been explored for TBCs, and many are still being considered, but the current industry standard in gas turbines is ZrO_2 - 7-8wt%Y_2O_3, ie yttria-stabilised zirconia (YSZ), deposited either by PS or PVD. In both cases, the porosity level is typically around 10-15%. Sprayed TBCs tend to have somewhat lower conductivities (typically quoted as ~1 $W\,m^{-1}\,K^{-1}$, ie about 40% of the value for fully dense tetragonal polycrystalline YSZ, which is reported [45, 46] to be ~2.5 $W\,m^{-1}\,K^{-1}$ at room temperature and to fall progressively to ~2.0 $W\,m^{-1}\,K^{-1}$ at high temperatures [47]). However, coatings produced by PVD are usually regarded as mechanically more stable. Sprayed coatings are typically ~ 0.3-0.8 mm in thickness, while those produced by PVD would commonly be ~ 0.2-0.5 mm. Of course, PVD is a slower and more expensive process than plasma spraying.

There has been extensive study [31, 48-54] of microstructural features exhibited by PS YSZ and of changes induced under service conditions [26, 55, 56]. The main features are a series of interfaces parallel to the plane of the coating (normal to the heat flow direction), representing boundaries between the splats formed from incident molten droplets. These interfaces are often rather poorly bonded and the associated thin gaseous layers between splats reduce the through-thickness conductivity. Fine columnar grains form during solidification, aligned normal to the plane of the coating. There has also been study [57-59] of radiation transmission characteristics. The material is relatively transparent to wavelengths in the near infra-red, although this radiation is strongly scattered by interfaces and grain boundaries.

3.2 Conduction through Gas in Pores

The thermal conductivity of a gas, K_g, in a constrained channel of length d_v can be estimated using the empirical expression [60]

$$K_g = K_g^0 \left(1 + \frac{4\gamma}{\gamma+1} \frac{2-A}{A} \frac{\lambda}{d_v \,\mathrm{Pr}} \right)^{-1} \qquad (2)$$

where K_g^0 is the unconstrained conductivity of the gas at the temperature concerned, $\gamma = C_p/C_v$ is the specific heat ratio, A is the accommodation coefficient (A~1 for TBCs [7]), Pr is the gas Prandtl number and λ is the mean free path of gaseous atoms or molecules. Assuming ideal gas behaviour for the mean free path [61], $\lambda \sim T/P$, where P is the pressure and T is the absolute temperature, allowing Eqn.(2) to be rewritten in more convenient form [60]:

$$K_g = \frac{K_g^0}{1 + B\,T\,/\,(d_v P)} \qquad (3)$$

where B is a constant which generally depends, not only on the gas type, but also on the solid surface material, surface roughness and gas-solid interactions [7, 35]. The value of B depends on the type of gas and several approximations have been suggested [7, 60, 62]. Substituting $\lambda = 60$ nm for air and $\lambda = 72$ nm for argon, at room temperature and atmospheric pressure, in Eqn.(2) leads to [61, 63] B~6.6 10^{-5} Pa m K^{-1} for air and 8.5 10^{-5} Pa m K^{-1} for argon. There are analytical expressions available for K_g^0 as a function of temperature, but in practice it is usually preferable to use experimental data. Fig.3 shows measured values for K_g^0 of air [64], together with predicted values of K_g, as a function of temperature and pressure, for a pore thickness of 100 nm. It can be seen that both temperature and gas pressure have significant effects. In this context, it may be noted that the pressure in the vicinity of a turbine typically varies between atmospheric and 40 bar. Furthermore, the gas permeability of TBCs is known [65, 66] to be high, so that such pressures will quickly become established throughout most of the pores within a coating. At atmospheric pressure, d_v is less than λ, and Knudsen heat transfer is operative in pores. This gives a weak dependence of K_g on temperature - see Fig.3. However, at P~40 bar, $d_v >> \lambda$ and K_g rises to a value similar to that in free air, K_g^0. In fact, experimental measurements of the thermal conductivity of TBCs are normally carried out at atmospheric pressure or below (ie with higher λ), in which case the conductivity of gas in the pores will be appreciably lower. Furthermore, measurements are often made only at room temperature, also giving lower conductivities. For example, at $T = 300$ K and $P = 0.01$ bar, the conductivity of air within fine pores is ~8 10^{-5} W m^{-1} K^{-1}, whereas at $T = 2000$ K and $P = 40$ bar it is ~0.1 W m^{-1} K^{-1}. Such differences turn out to have substantial effects on the overall conductivity of the TBC – see §3.4 below.

3.3 Radiative Heat Transfer

Depending on the temperature and scattering characteristics, radiative heat transfer can be significant in gases and translucent solids. The interaction of radiation with a thermal field is complex and coupled conduction-radiation transport equations [32] should be solved. However, by averaging the wavelength dependence of absorption (κ) and scattering (β) coefficients, and assuming isotropic scattering, approximations (particularly the Milne-Eddington approximation) describing the overall 1-D heat transfer can be made [32, 67]. According to this approximation, the radiation flux falls to about e^{-1} of its initial value within a radiation decay distance $L_r \sim (3\kappa\alpha)^{-0.5}$, in which α ($= \beta+\kappa$) is an extinction coefficient. The incident beam intensity decays more rapidly than this, since the scattering distance for radiation is α^{-1}. However, when radiation inside a TBC becomes diffused, there is a certain amount of re-emission and it is reasonable to treat L_r as a characteristic length for decay of the net radiative flux.

The heat flow in TBCs is not unidirectional. The process is complex and has 3-D geometry. However, a diffusive approximation (with the radiative contribution to overall heat transfer

characterised by a "conductivity" which is added to that from conduction) is appropriate in certain cases. The first is under conditions of strong absorption, in which case K_{rad} is given by

$$K_{\mathrm{rad}} \approx \frac{16n^2}{3\alpha}\sigma_{\mathrm{SB}}T^3, \qquad (4)$$

in which σ_{SB} is the Stefan-Boltzmann constant and n is the refractive index. The value [57] of n for PS YSZ, in the wavelength range of interest, is ~2.1. Radiative heat transport is in general the outcome of multiple scattering and absorption events, as well as direct radiative transfer. It can be shown [32] that, under strong absorption conditions, the net flux is controlled by the extinction coefficient α, and not by L_r. Furthermore, free surface and interface boundary conditions are not relevant to Eqn.(4), since it relates to a region of thickness L_r, which is much smaller than the coating thickness, H.

The second case is when there is very little absorption. In this case, radiation does not "sense" the local temperature field and the radiative heat flux can be completely separated from that due to conduction. Boundary conditions play a role in conduction if α^{-1} is smaller than H. In this case Eqn.(4) should be modified.

$$K_{\mathrm{rad}} \approx \frac{4n^2}{\left(3\alpha/4 + H^{-1}(\varepsilon_t^{-1} + \varepsilon_b^{-1} - 1)\right)}\sigma_{\mathrm{SB}}T^3 \qquad (5)$$

where ε_t and ε_b are absorptivities of top and bottom surfaces respectively. This equation is expected to be valid is valid if $H<L_r$. Otherwise, the radiation starts to couple with the conduction [67].

The absorptivity [68] of YSZ is approximately constant ($\kappa \sim 10\ \mathrm{m}^{-1}$) over the range $T \sim 300$-1300 K, but rises sharply [69-71] to $\kappa \sim 2\ 10^3\ \mathrm{m}^{-1}$ as the temperature is raised to 2000 K. The scattering coefficient for PS YSZ has been estimated [59] as $\beta \sim 5\ 10^4\ \mathrm{m}^{-1}$ for $\lambda = 2\mu$m. Since n is unlikely to vary much with temperature [72], β is a function of pore size only, and is temperature-independent.

Predictions from these equations are summarised in Fig.4. Fig.4(a) shows the radiation decay length L_r, as a function of T, for PS YSZ, before and after a substantial heat treatment. Sintering effects (see §4) are likely to decrease β and increase L_r. The scattering length β^{-1} for PS YSZ is thus expected to be higher after sintering, and has been reported [68, 70] to reach about 50 μm after extensive heat treatment. At low temperatures (<1500K), radiation transfers heat directly through the coating, whereas at higher temperatures absorption and re-radiation inside the coating play an increasing role, and Eqn.(4) should be used. The radiative conductivity at high temperatures is thus as shown in Fig.4(b), for different scattering lengths, which will in turn be a function of grain size. It can be seen that the radiative contribution starts to become significant for temperatures above about 1500 K. At 1500 K, $K_{rad} \sim 0.05$-$0.1\ \mathrm{W\ m^{-1}\ K^{-1}}$, whereas at 2000 K it could [16, 45] raise the conductive value (~1 $\mathrm{W\ m^{-1}\ K^{-1}}$) by over 20%. Furthermore, this would rise to a 50% increase if the radiative decay distance were to be increased to 50 μm, which could occur as a result of extensive sintering. Clearly, the insulating capacity of a coating is thus likely to be significantly reduced if the temperature is very high and/or extensive sintering has occurred.

3.4 Overall Conduction through TBCs – the "Two Flux Regimes" Analytical Model

In order to incorporate the effects of both heat transfer through the gas in pores, and within the zirconia itself, and also the architecture of the pores, some kind of simulation is required of the

geometric arrangement, and the way that heat flows through it. Such a model was presented recently by Golosnoy et al [15]. The basis of this model (in which the proportionate area of a splat in contact with its neighbours is an important parameter) is illustrated in Fig.5. The main feature is division of the overall heat flux into two regimes, one in which conduction occurs through the contact "bridges" between adjoining splats, with some "funnelling" of heat flow towards these regions of low thermal resistance, and one involving unidirectional conduction successively through the splats and the intervening air gaps. The width of the "funnelled" zone is found by establishing the value giving the highest overall rate of heat transfer – see Fig.5. Implementation of the model involves use of some simple analytical equations. As can be imagined, depending on the ratio of the conductivities of gas and solid, the predicted value [15] of the effective conductivity is sensitive to the relative area of bridged contact A_{br}/A_{tot}. The two micrographs shown in Fig.5, taken before and after a heat treatment, illustrate how this contact area can rise sharply as a consequence of sintering effects – see §4 below.

Some predictions from this model are shown in Fig.6, together with experimental data from Ratzer-Scheibe et al [73, 74]. The spraying conditions, and coating microstructures, were similar to those reported elsewhere [31, 75-77]. The predictions shown were obtained using input data, and predictions from the sintering model, shown in Table I. The experimental measurements were made in vacuum, and under 1 bar of argon, on PS YSZ TBCs given a prior heat treatment. It can be seen in Fig.6 that agreement between measured and predicted data is good in terms of absolute magnitude, dependence on temperature and the effect of the presence of the argon. The figure also illustrates the fact that significant increases in effective conductivity are predicted to arise from the presence of gas (air) under high pressure within the pores. For example, it's predicted that, at 1500 K, this would cause the effective conductivity to rise from ~1.1 W m^{-1} K^{-1} to ~1.4 W m^{-1} K^{-1}. Unfortunately, there are virtually no experimental data available in the open literature for TBC conductivities measured under these high gas pressures, and in general the equipment used is not suitable for such testing. Nevertheless, these are the conditions under which gas turbines normally operate. It's therefore clear that further work is needed in this area. It is also clear that sintering, which can certainly occur under service conditions, raising both the inter-splat bridge area and the grain size (and hence the radiation decay distance, L_r), can significantly increase the overall conductivity (see §4.2).

4 Sintering in TBCs

It has become clear that one of the main factors limiting the performance of TBCs (both PS and PVD) is the tendency for deleterious microstructural changes to occur during prolonged exposure to high temperature. In general, these changes tend to cause reduced thermal insulation capacity [16-18, 78] and reduced strain tolerance [19-21, 26, 79, 80], both of which are highly undesirable. It's also clear that sintering can be accelerated by the presence of species that become concentrated in grain boundaries or at free surfaces, whether present as impurities in the coatings [31] or as material absorbed during turbine operation [27-30]. Species that dissolve in the lattice, on the other hand, such as alternative stabilisers to yttria, tend to have little effect on the sintering characteristics [78].

Unfortunately, while the most productive strategy for minimisation of the thermal conductivity of PSZ TBCs has been to create a fine scale microstructure and pore architecture, with multiple interfaces, all offering thermal resistance, one consequence of this is that the diffusion distances required for sintering and microstructural coarsening are relatively short, so that it tends to occur readily at relatively moderate temperatures. Moreover, these fine microstructures and pore architectures offer considerable scope for diffusion to occur via grain boundaries and free surfaces,

where species can migrate much faster than within the lattice. As a consequence, sintering-induced changes can occur fairly quickly in TBCs at temperatures as low as ~1100˚C, which represents an homologous temperature of less than 0.5. It's therefore very important that these sintering pheneomena (in TBCs, under turbine operating conditions) should be well understood. This should assist considerably in devising approaches to minimising the associated deleterious effects.

4.1 Modelling of Changes in Pore Architecture

Several models have been developed for simulation of sintering in TBCs, mostly based on the variational principle [81-84] - ie microstructural evolution is assumed to occur along a path which optimises the rate of net energy reduction. In particular, Cipitria et al [77, 85] have recently published a model for sintering of PS YSZ TBCs, including simulation of the effects of attachment to a substrate [85]. The basic geometry of the system, which is illustrated in Fig.7, is similar to that used for simulation of heat transfer [15], although the model actually incorporates different domain structures for growth of the inter-splat contact area and for healing of the intra-splat microcracks. A compiled version of the code for implementation of the model is available for downloading [77].

Fig.8 shows predicted and measured dimensional changes taking place in free-standing PS YSZ TBCs during heat treatments. The agreement is good and such shrinkage is important and informative. However, it should be noted that it arises solely from grain boundary diffusion, since surface diffusion generates no volume change and lattice diffusion is negligible in these TBCs over the temperature range of interest. In fact, it is in many ways the surface diffusion that has the predominant effect during these heat treatments [77], particularly concerning growth of inter-splat "bridges". There are measurable parameters that are sensitive to surface diffusion, such as the specific surface area, and comparisons between predicted and measured values of this also show good agreement [77, 85]. Attempts to reduce the deleterious effects of sintering in TBCs should probably be focussed largely on surface diffusion and on possible approaches to reducing surface diffusivities or affecting surface diffusion pathways.

4.2 Predicted Changes in Conductivity

It's already well-established that substantial microstructural changes can be induced in YSZ TBCs (PS and PVD) by heat treatments of the type commonly imposed under service conditions. It's also clear that these changes lead to increases in (effective) thermal conductivity (and also in stiffness). Since the sintering model of Cipitria et al [76, 77, 85] is based on much the same geometrical model as that of Golosnoy et al [15] for prediction of conductivity, and also involves similar microstructural characterisation parameters, it's possible to combine them in order to predict how the conductivity changes during heat treatment. For example, Fig.9 compares such predictions with experimental data from Ratzer-Scheibe et al [73, 74], relating to PS YSZ TBCs given short or prolonged heat treatments at 1100˚C. The microstructural and architectural parameters used in obtaining these model predictions are shown in Table I. It can be seen that agreement is again good. It's also clear that, even at a temperature as low as 1100˚C, prolonged exposure can lead to an increase in conductivity of the order of 50% (from ~0.7 $W\,m^{-1}\,K^{-1}$ to ~1.0 $W\,m^{-1}\,K^{-1}$). In contrast, the associated changes in overall porosity level are very small - less than 1% (Table I). This is an additional indication that the overall porosity level is not a suitable parameter for characterisation of the microstructure or prediction of any of the relevant properties.

A similar comparison between predicted and measured conductivity data is shown in Fig.10, with the measurements in this case being made at room temperature and the data plotted against the time

of exposure to a temperature of 1400˚C. It can be seen that, at this temperature, the rise in conductivity is rapid and becomes significant in a few hours. It's also clear from the difference between predictions obtained using the monodisperse pore size (125 nm) and the bimodal size distribution that the details of the pore architecture can have a significant effect on the kinetics of sintering. In this case, having some fine pores (very small inter-splat spacings) accelerates the initial rate of growth of the contact bridges, and hence the rate of increase of the thermal conductivity, quite substantially, even if the average pore size remains the same.

It may be noted that the predictions shown in Fig.10 are based on the assumption that only the tetragonal phase was present. In fact, high purity specimens contain ~30% of cubic phase and <~1% monoclinic phase [75], even after 100 h at 1400˚C. In fact, the difference between the conductivities of the tetragonal and cubic phases in this system is relatively small [46, 47] and can be neglected for most purposes.

Also evident in this plot is that experimental conductivity data for TBCs can show quite a lot of scatter. This isn't so evident in experimental data like those shown in Figs.6 and 9, which relate to a particular specimen located in a (laser flash) experimental facility, being tested in an identical way after repeated increases in temperature. However, when measurements are made in one-off operations on different specimens, and using different experimental facilities and methods, then substantially greater scatter is in general observed. For example, the data shown in Fig.10 were obtained using both steady state [86] and transient [87] techniques. Furthermore, TBCs produced under slightly different conditions can exhibit significantly different microstructures, and there can even be variations between different parts of the same coating. It's certainly clear from the sinter modelling work [77, 85] that the behaviour is very sensitive to the details of the (initial) pore architecture. This can make it difficult to compare absolute values of conductivity obtained by different research groups, or during different experimental programmes, although of course it's still possible to identify important trends and effects.

Finally, it's worth noting that most experimental work of this type is carried out on coatings that have been detached from their substrates and are subjected to isothermal heat treatments. Under service conditions, on the other hand, coatings remain attached to metallic substrates and are repeatedly subjected to high thermal gradients and rapid cooling and heating cycles. In fact, Cipitria et al have shown [85] that attachment to a substrate does not strongly affect the way that sintering occurs at high temperature, apart from inhibiting the in-plane shrinkage, since stress relaxation occurs very rapidly. However, rapid heating and cooling cycles, while deleterious because they can lead to high internal stresses, which may promote debonding and spallation, could retard sintering by generating local stresses which fracture growing necks etc. There are some limited results available [78] which suggest such an effect.

5 Conclusions

The following conclusions can be drawn from this work.

(a) This review covers heat flow through plasma sprayed, zirconia-based, thermal barrier coatings, with reference to the conditions they commonly encounter during operation of gas turbines. This can involve exposure to high velocity gas, at temperatures up to around 1750 K, with strong interest in the turbine entry temperature being raised even further. There is enormous incentive to maximize the thermal protection offered by TBCs, while minimizing their thickness and mass, so a low overall conductivity is required, preferably below about 0.5 W m^{-1} K^{-1}. Figures of this order are often quoted for plasma sprayed TBCs, but in reality the true value under operating conditions is often appreciably higher.

(b) These coatings are relatively porous, and heat transfer through them is very sensitive to the details of the pore architecture. Heat transfer takes place mainly via conduction, although the contribution from radiation can become significant at temperatures above about 1500 K. The details depend on radiation scattering lengths, which rise as the grain structure coarsens and inter-splat contact area increases.

(c) The conduction takes place through solid zirconia and through gas-filled pores, particularly in the form of thin gaps between overlaying splats. The conductivity of gas in these pores has quite a strong influence on the overall heat transfer. It is lower than that in corresponding free gas, as a result of mean free path effects in a constrained channel. Provided the pressure is around atmospheric or below, the conductivity remains low over the complete temperature range. However, when the gas pressure is high (~40 bar), as it commonly is during turbine operation, its conductivity within these pores can be considerably higher, particularly at high temperature. The effect of a high gas pressure is of particular concern, since very few experimental measurements of conductivity have been made with such pressures being applied.

(d) One of the main areas of concern with TBCs (both plasma sprayed and PVD) relates to the changes in microstructure and pore architecture that tend to take place under turbine operating conditions as a consequence of sintering effects. These can coarsen the microstructure and generate improved contact between overlapping splats, both of which tend to raise the conductivity. The mechanisms and characteristics of sintering under these conditions are becoming better understood and some modelling results are presented to illustrate these. Improved control of sintering effects is an important aim for current research efforts.

Acknowledgements

Financial support has come from a Basque Government scholarship (for AC), from EPSRC via a Platform Grant (for IOG) and from Sulzer Metco (US) Inc. There has been extensive technical collaboration with Sulzer Metco, particularly Mitch Dorfman , Clive Britton and Steve Bomford.

Tables

Variable	Source	Input data for sintering model	Predictions from sintering model	
			After 2 hours	After 100 hours
Height of cell	[77]	2.626 μm	2.625 μm	2.624 μm
Width of conductivity modelling cell	[77]	5.32 μm	5.32 μm	5.32 μm
Radius of sintering modelling cell	[77]	3.00 μm	3.00 μm	3.00 μm
Grain size	[77]	0.50 μm	0.50 μm	0.50 μm
Opening dimensions of (inter-splat) pores	[23, 31, 80, 88, 89]	125 nm	128 nm	145 nm
Inter-splat contact area, A_{br}/A_{tot}	[48]	15%	17.3%	27.4%
Inter-splat porosity level	[51, 90]	4.05%	4.04%	4.01%
Globular porosity level	[51, 90]	6.00%	6.00%	6.00%

Table I Input data for and predictions from the sintering model [77]. Predictions were used as input data for the conductivity model [15].

Figure Captions

Fig.1 *Schematic representation of heat transfer mechanisms in zirconia-based plasma sprayed TBCs.*

Fig.2 *Predicted (Eshelby method) dependence of thermal conductivity (as a ratio to that of the matrix) on: (a) void content and shape (s is the aspect ratio of insulating, oblate ellipsoidal inclusions) and (b) void content only, for spherical inclusions, plotted together with approximate experimental data for a wide selection of highly porous materials.*

Fig.3 *Predicted effect of temperature and pressure on the thermal conductivity of air in pores with a thickness of 100 nm; the experimental data of Incropera and DeWitt [64] for the conductivity of free air, which are also shown in the plot, were used as a base for the predictions.*

Fig.4 *Predicted dependence on temperature of (a) net radiation absorption distance, L_r, and (b) radiative thermal conductivity.*

Fig.5 *Schematic representation of the "two flux regimes" model [15] for heat flow through a set of plates connected via bridges, together with SEM micrographs of PS YSZ, before and after a heat treatment of 50 hours at 1300˚C.*

Fig.6 *Comparison between experimental data of Ratzer-Scheibe et al [73, 74] and predictions from the model of Golosnoy et al [15], for the dependence of the measured (effective) conductivity of PS YSZ TBCs on temperature. The specimens had been given a prior heat treatment at 1100˚C for 100 h. Input data used are given in Table I.*

Fig.7 *Schematic representation of the diffusional migrations, and consequent morphological changes and associated macroscopic shrinkages, that occur during sintering of PS TBCs, according to the model of Cipitria et al [77, 85].*

Fig.8 *Comparison [77] between experimental data and model predictions for coating shrinkage, (a) at 1400˚C in both through-thickness and in-plane directions and (b) in the through-thickness direction, at both 1200˚C and 1400˚C.*

Fig.9 *Comparison between experimental data of Ratzer-Scheibe et al [73, 74] and predictions from the model of Golosnoy et al [15], for the dependence of the measured (effective) through-thickness conductivity of PS YSZ TBCs on temperature and on prior heat treatment. These measurements, which were carried out in vacuum, were made after specimens had been heat treated at 1100˚C for either 2 h or 100 h*

Fig.10 *Comparison [77] between experimental data and model predictions for the through-thickness thermal conductivity, as a function of the duration of a prior heat treatment at 1400˚C. The two predicted curves correspond to different assumptions about the range of values exhibited by the inter-splat spacings and the opening of the intra-splat microcracks.*

Figures

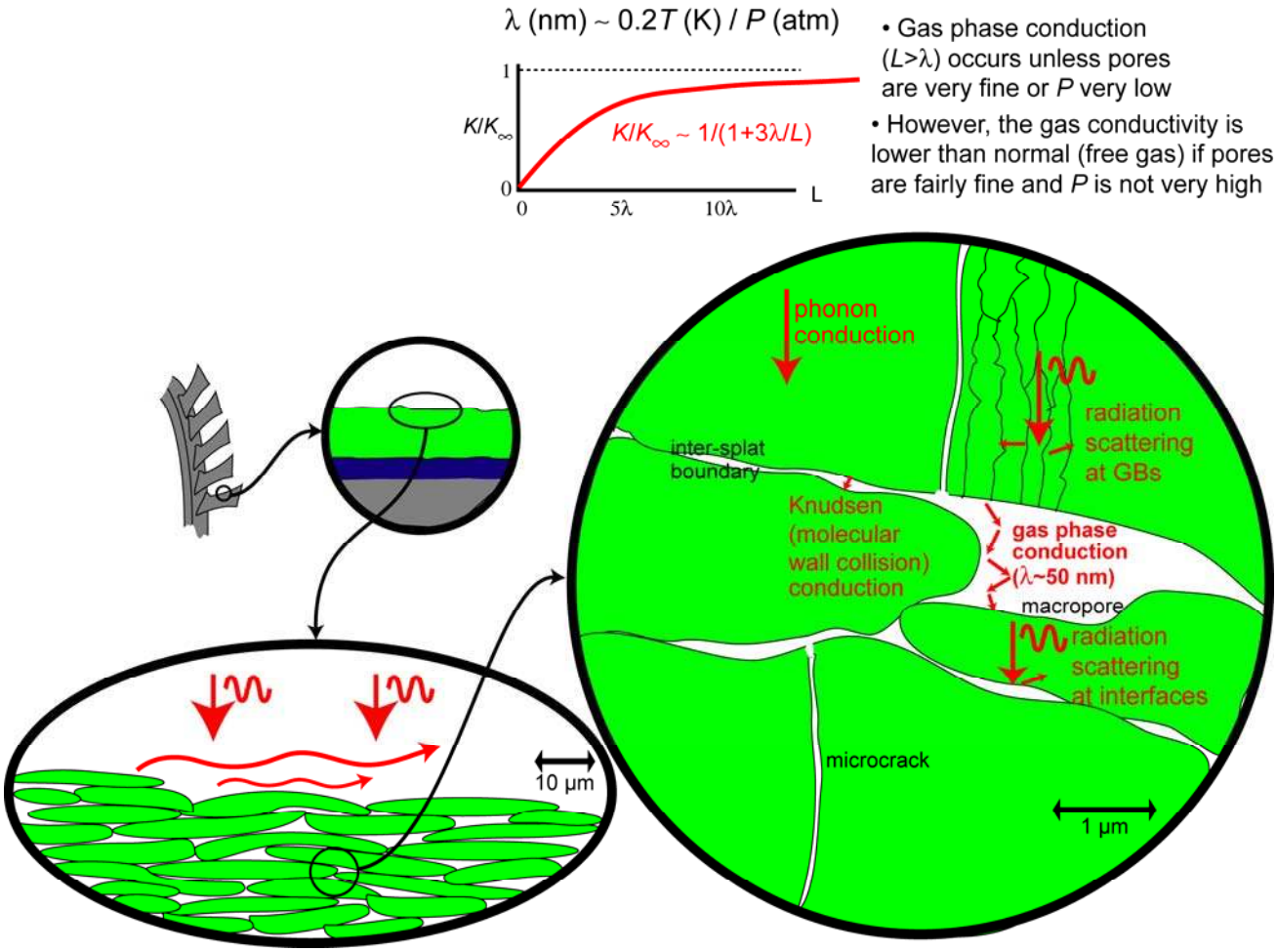

Fig.1 *Schematic representation of heat transfer mechanisms in zirconia-based plasma sprayed TBCs.*

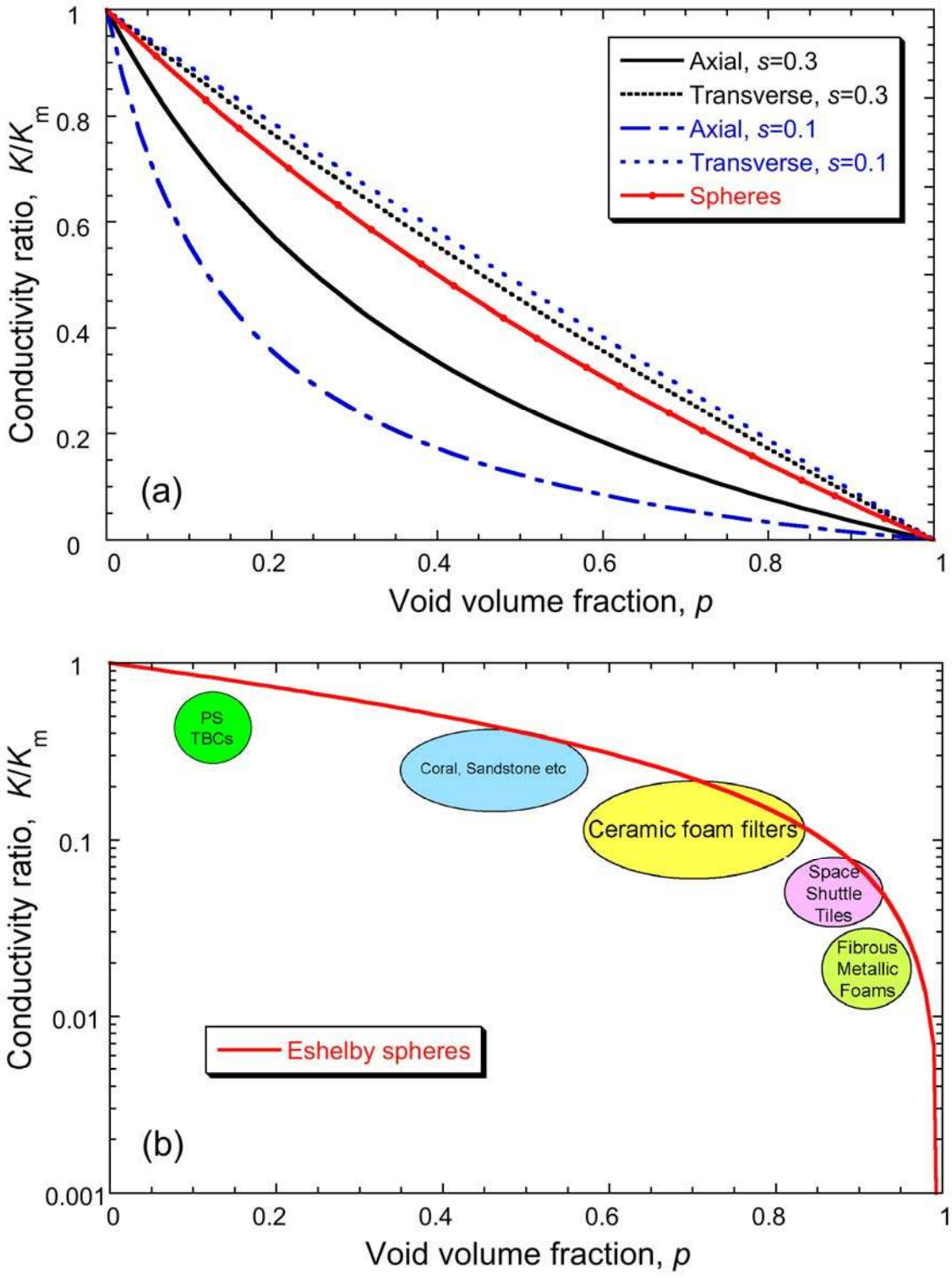

Fig.2 *Predicted (Eshelby method) dependence of thermal conductivity (as a ratio to that of the matrix) on: (a) void content and shape (s is the aspect ratio of insulating, oblate ellipsoidal inclusions) and (b) void content only, for spherical inclusions, plotted together with approximate experimental data for a wide selection of highly porous materials.*

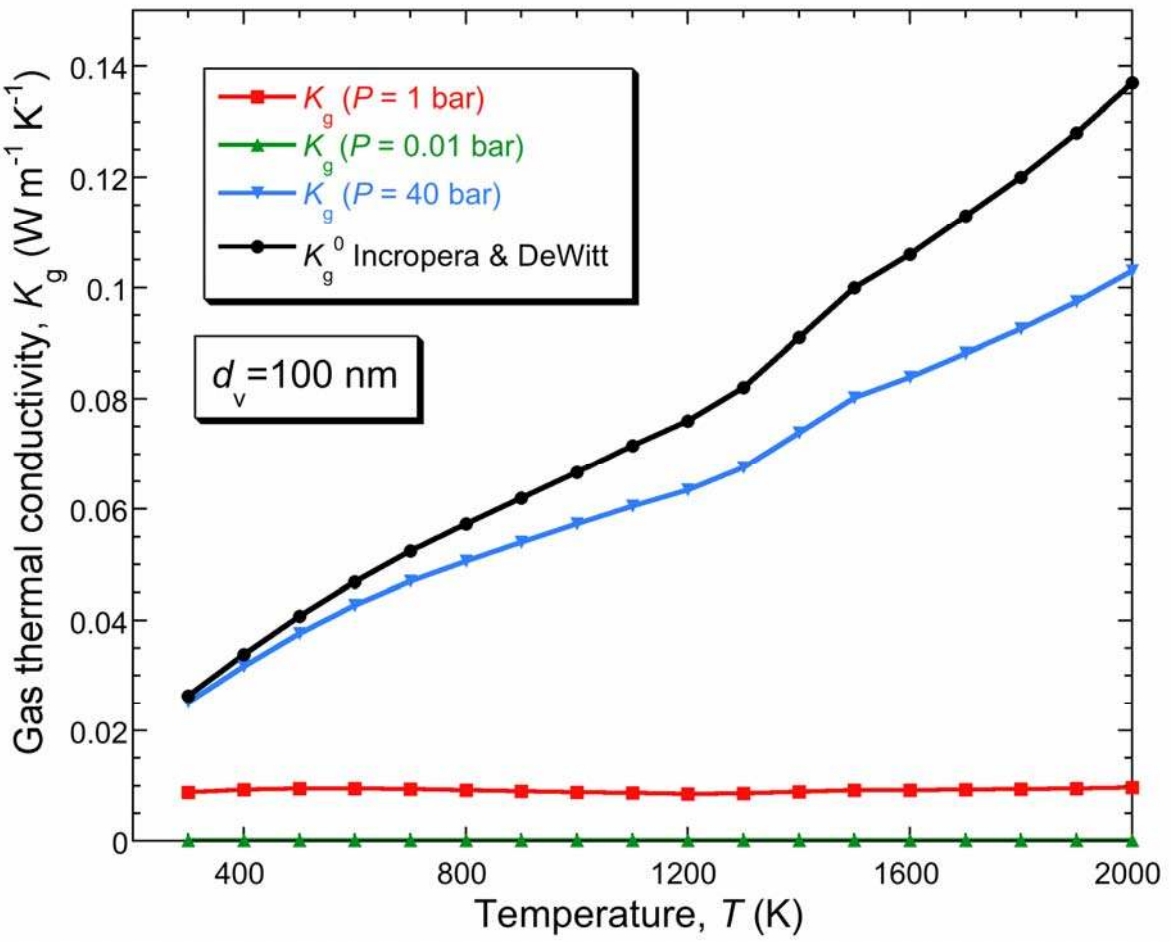

Fig.3 *Predicted effect of temperature and pressure on the thermal conductivity of air in pores with a thickness of 100 nm; the experimental data of Incropera and DeWitt [64] for the conductivity of free air, which are also shown in the plot, were used as a base for the predictions.*

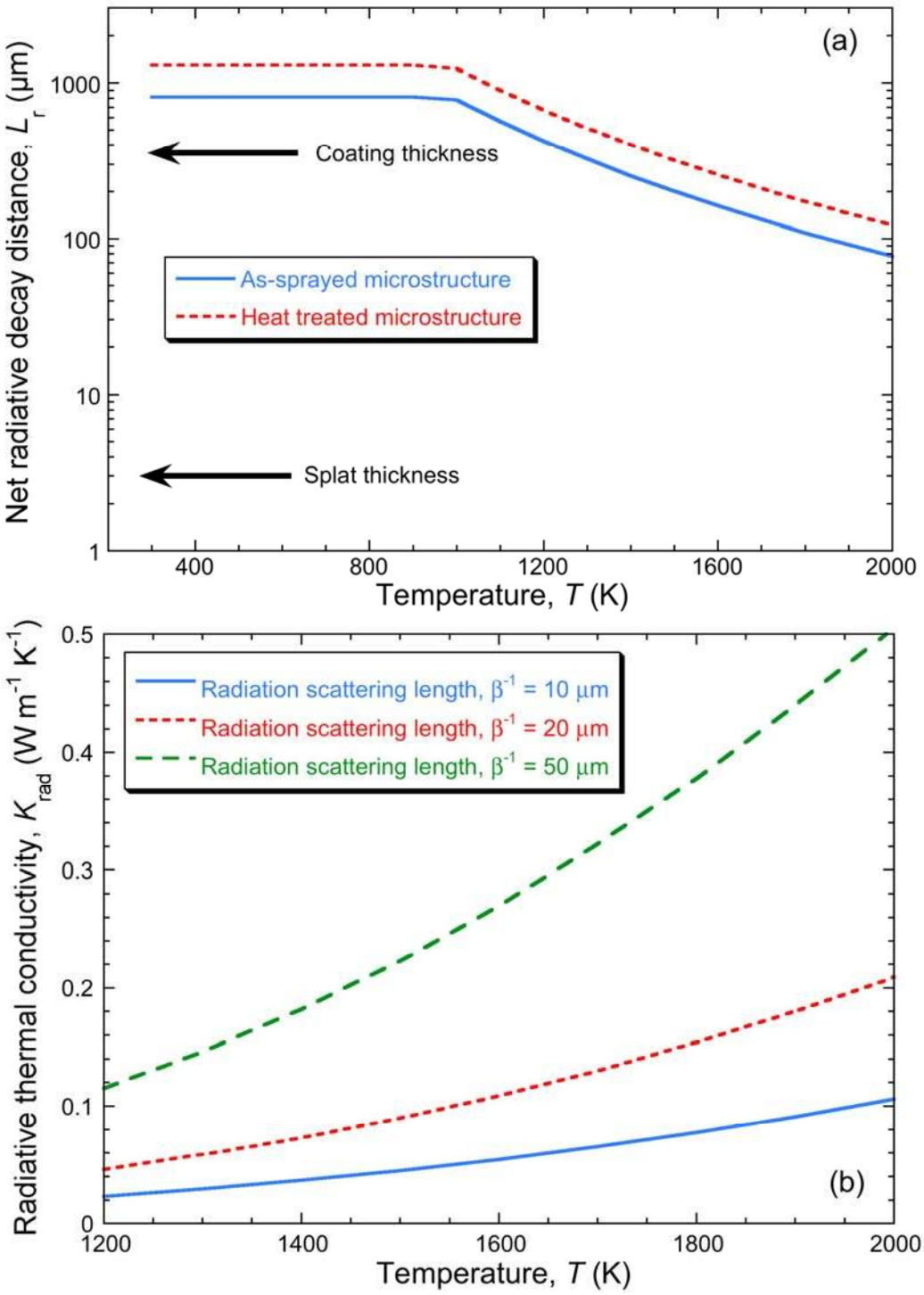

Fig.4 *Predicted dependence on temperature of (a) net radiation absorption distance, L_r, and (b) radiative thermal conductivity.*

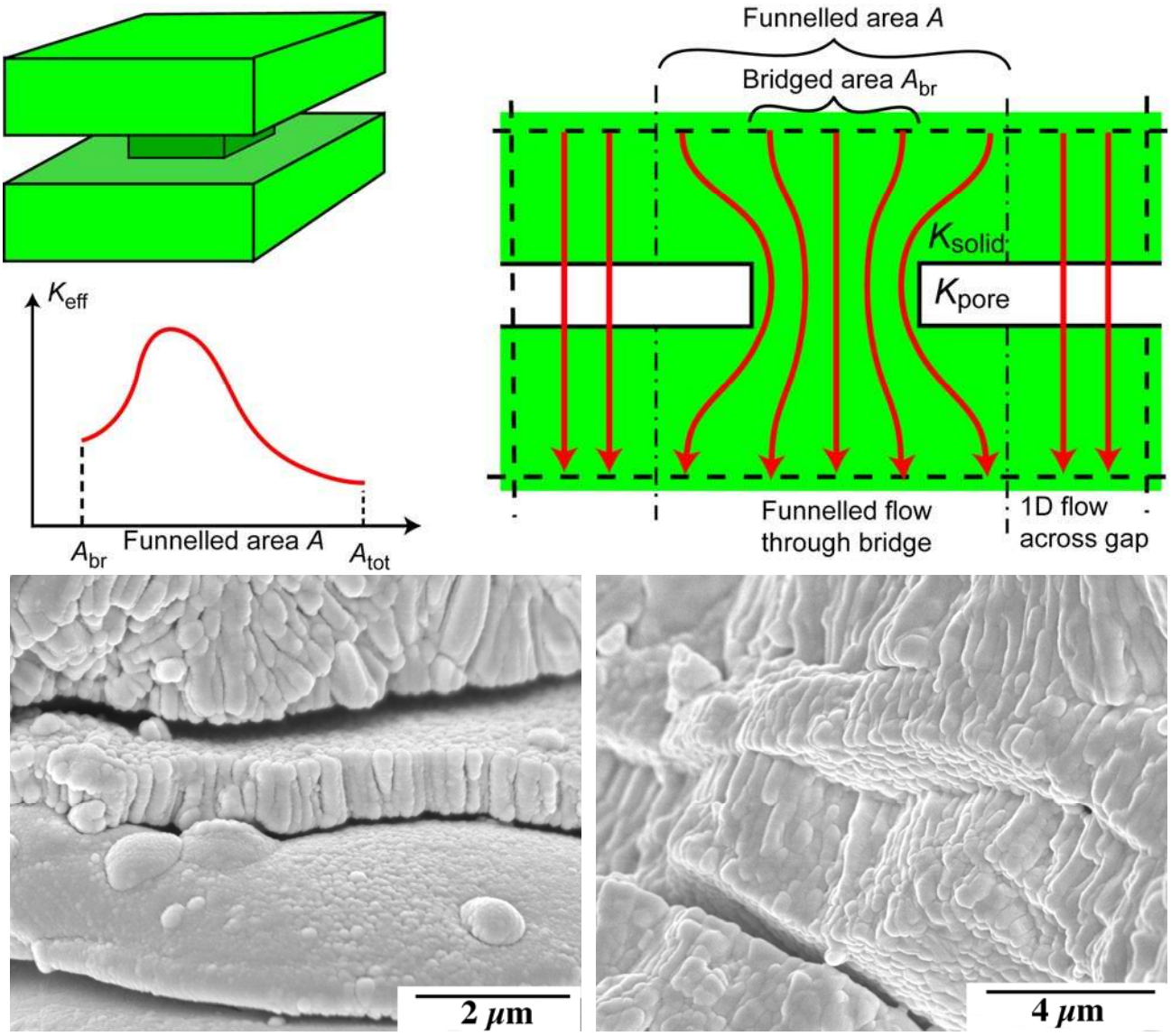

Fig.5 *Schematic representation of the "two flux regimes" model [15] for heat flow through a set of plates connected via bridges, together with SEM micrographs of PS YSZ, before and after a heat treatment of 50 hours at 1300˚C.*

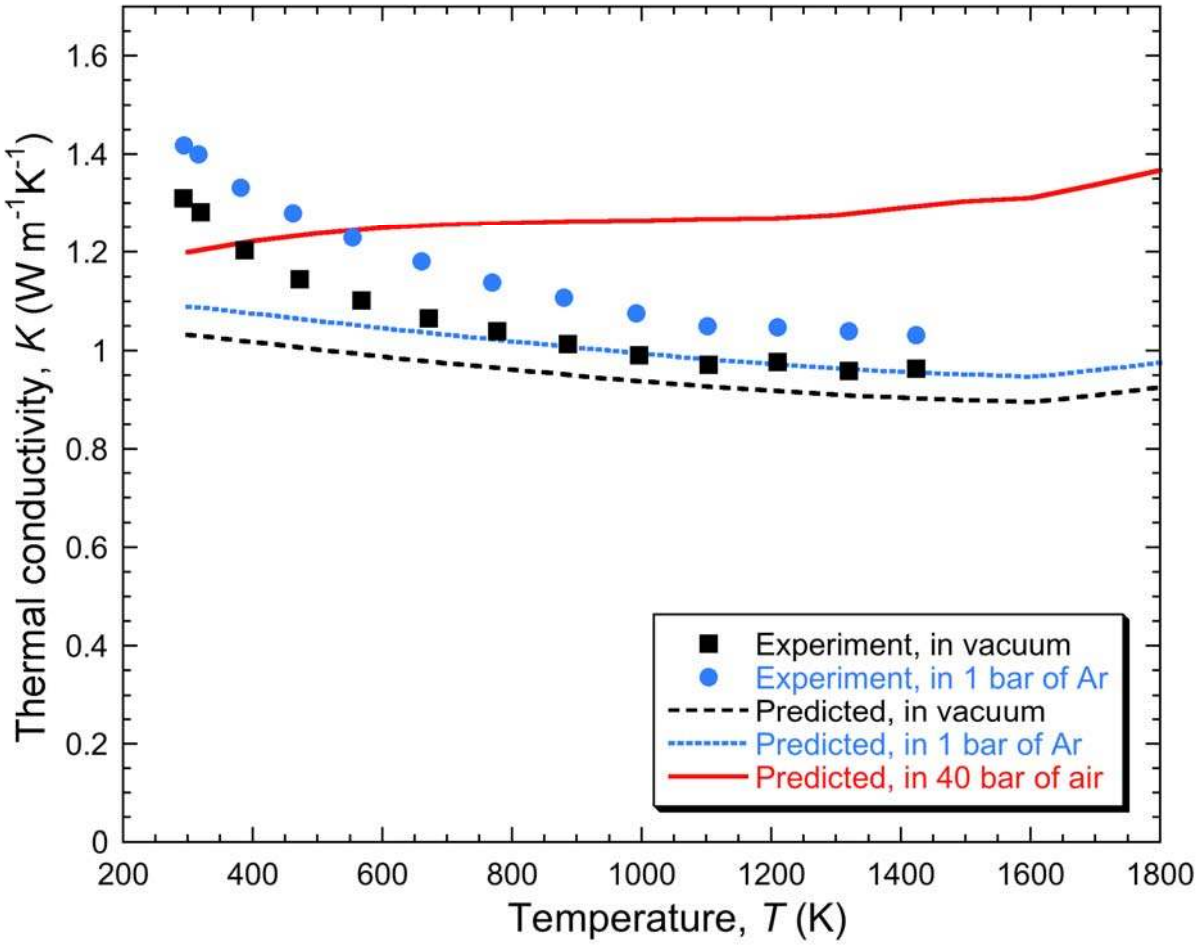

Fig.6 *Comparison between experimental data of Ratzer-Scheibe et al [73, 74] and predictions from the model of Golosnoy et al [15], for the dependence of the measured (effective) conductivity of PS YSZ TBCs on temperature. The specimens had been given a prior heat treatment at 1100˚C for 100 h. Input data used are given in Table I.*

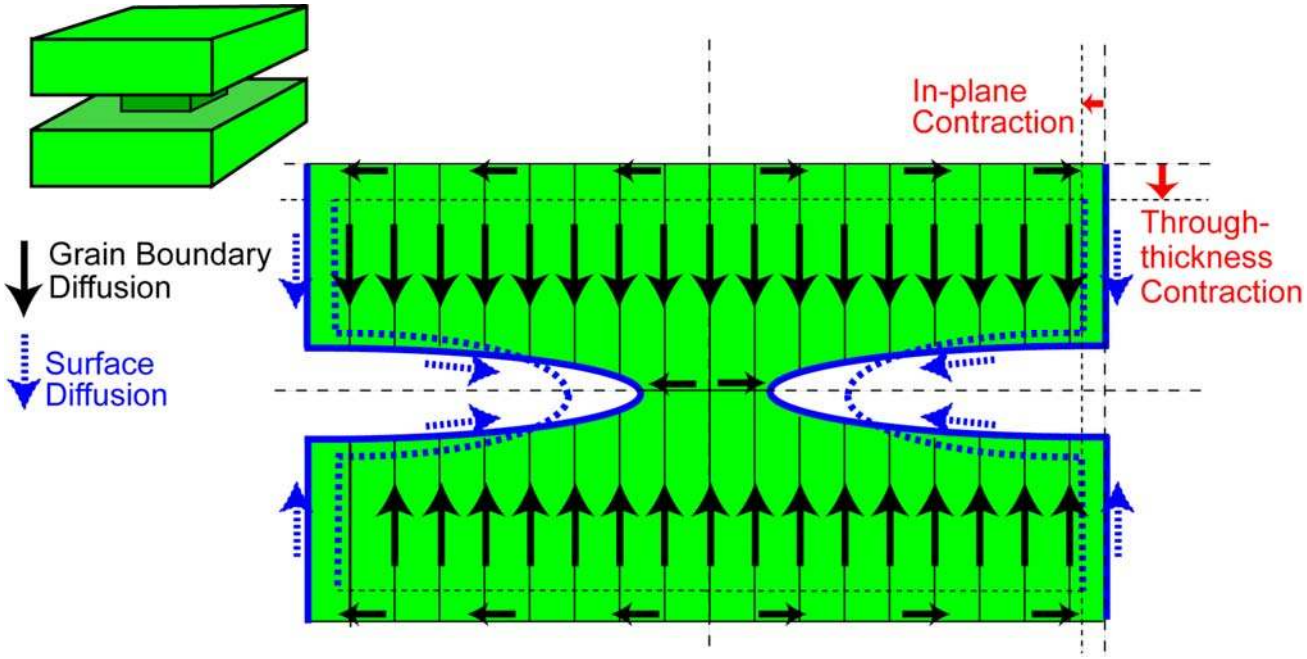

Fig.7 *Schematic representation of the diffusional migrations, and consequent morphological changes and associated macroscopic shrinkages, that occur during sintering of PS TBCs, according to the model of Cipitria et al [77, 85].*

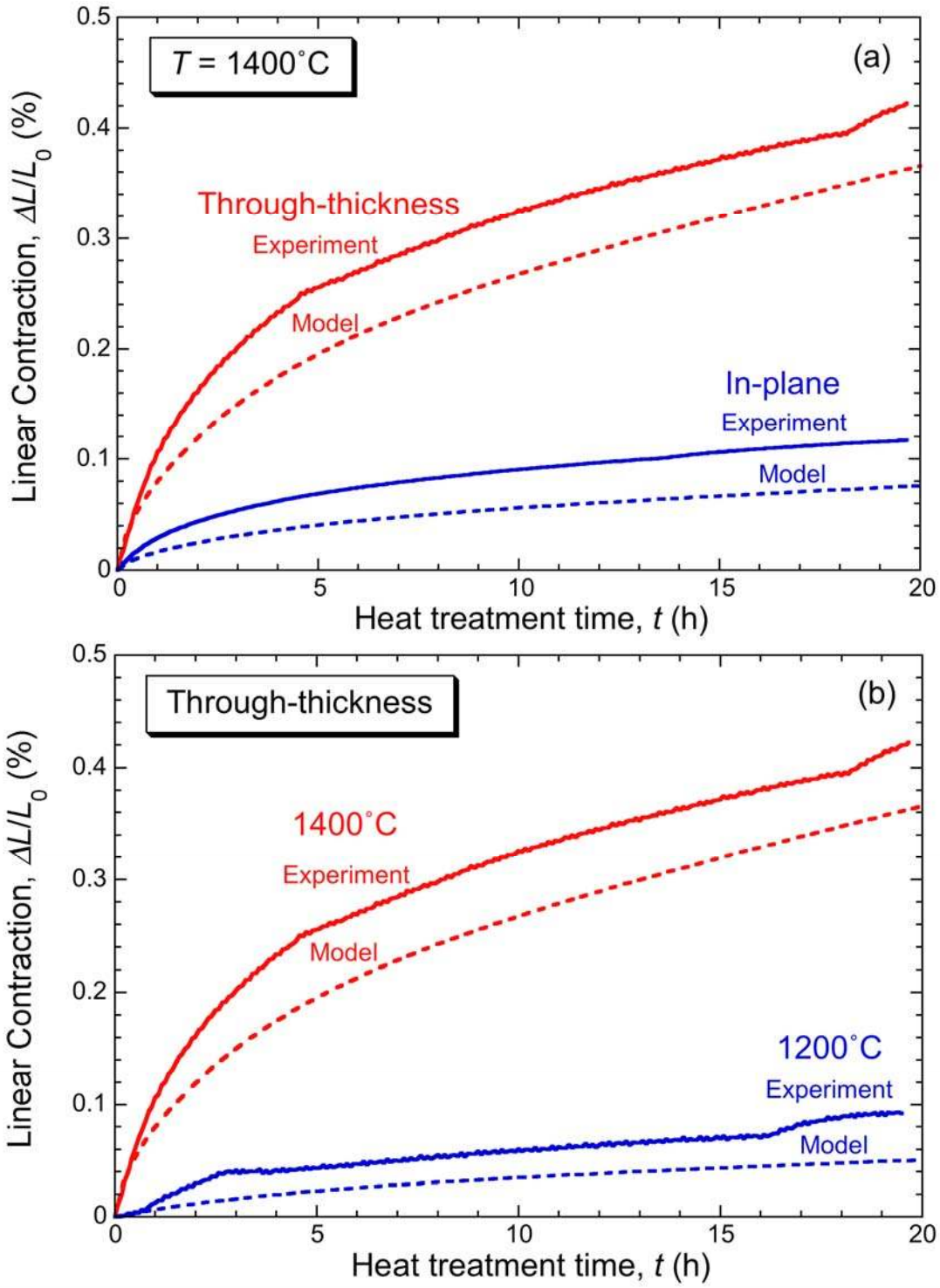

Fig.8 *Comparison [77] between experimental data and model predictions for coating shrinkage, (a) at 1400˚C in both through-thickness and in-plane directions and (b) in the through-thickness direction, at both 1200˚C and 1400˚C.*

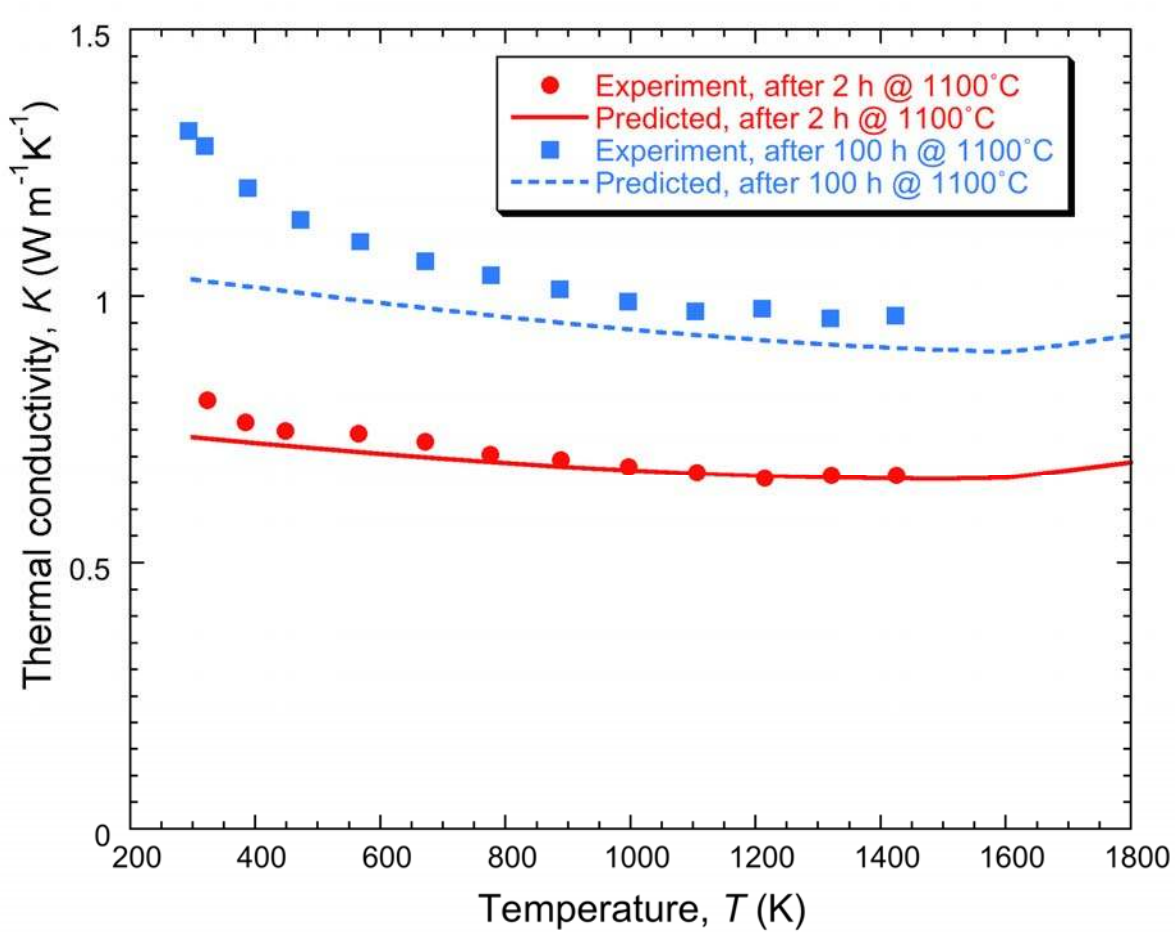

Fig.9 *Comparison between experimental data of Ratzer-Scheibe et al [73, 74] and predictions from the model of Golosnoy et al [15], for the dependence of the measured (effective) through-thickness conductivity of PS YSZ TBCs on temperature and on prior heat treatment. These measurements, which were carried out in vacuum, were made after specimens had been heat treated at 1100˚C for either 2 h or 100 h*

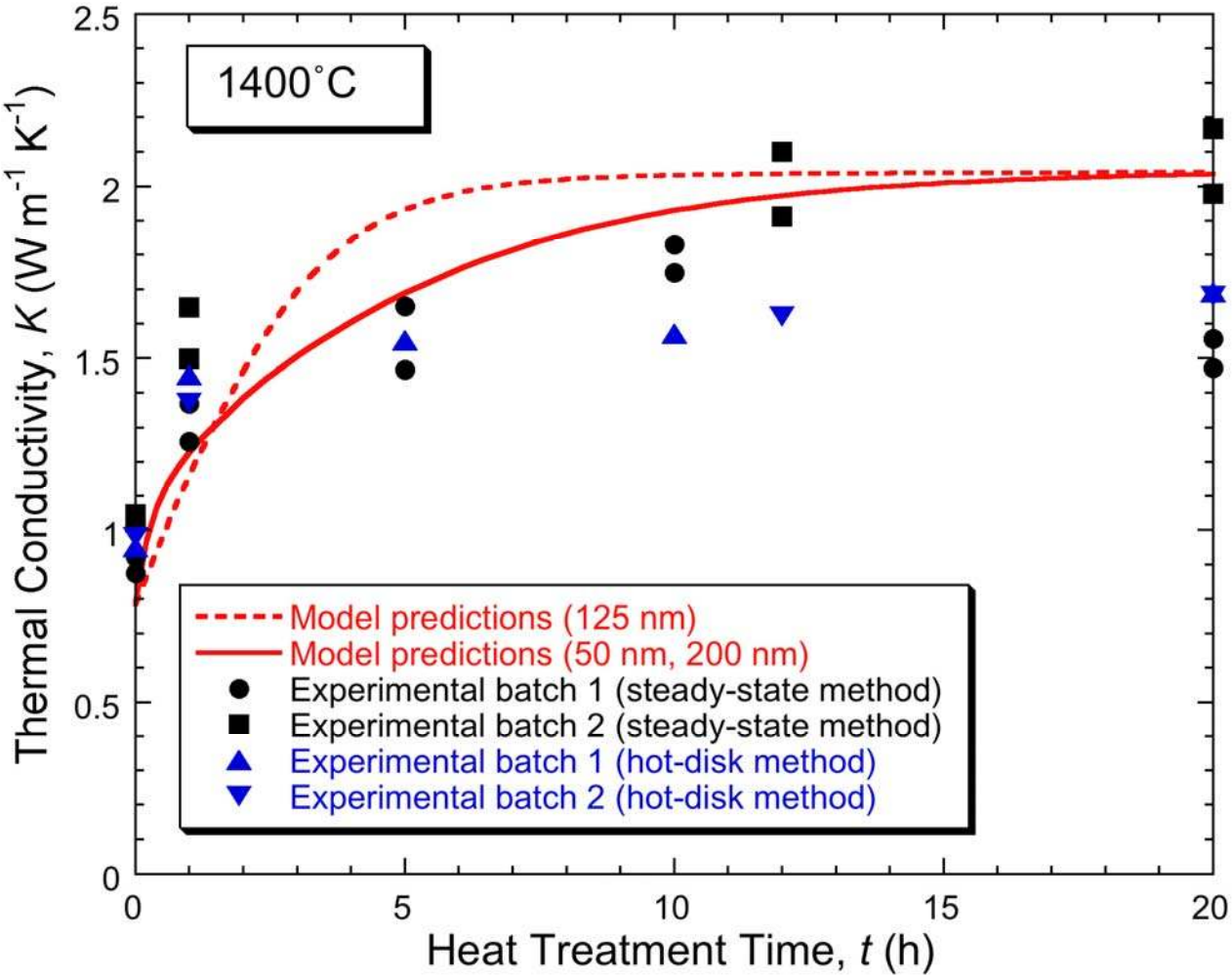

Fig.10 *Comparison [77] between experimental data and model predictions for the through-thickness thermal conductivity, as a function of the duration of a prior heat treatment at 1400˚C. The two predicted curves correspond to different assumptions about the range of values exhibited by the inter-splat spacings and the opening of the intra-splat microcracks.*

References

[1] T.W. Clyne, Thermal and Electrical Conduction in MMCs, in Comprehensive Composite Materials, Vol. 3 : Metal Matrix Composites, T.W. Clyne, Ed., Elsevier: Amsterdam, 2000, p. 447-468.

[2] T.W. Clyne, I.O. Golosnoy, J.C. Tan, and A.E. Markaki, Porous Materials for Thermal Management under Extreme Conditions, Phil. Trans. A: Math. Phys. Eng. Sci., 2006, 364(1838), p. 125-146.

[3] T.W. Clyne and P.J. Withers, An Introduction to Metal Matrix Composites, Cambridge Solid State Science Series, E. Davis and I. Ward, Eds., Cambridge: Cambridge University Press, 1993

[4] I. Sevostianov and M. Kachanov, Anisotropic thermal conductivities of plasma-sprayed thermal barrier coatings in relation to the microstructure, J. Therm. Spray Technol., 2000, 9(4), pp. 478-482.

[5] B. Shafiro and M. Kachanov, Anisotropic effective conductivity of materials with nonrandomly oriented inclusions of diverse ellipsoidal shapes, J. Appl. Phys., 2000, 87(12), pp. 8561-8569.

[6] F. Cernuschi, P. Bianchi, M. Leoni, and P. Scardi, Thermal diffusivity/microstructure relationship in Y-PSZ thermal barrier coatings, J. Therm. Spray Technol., 1999, 8(1), pp. 102-109.

[7] R. McPherson, A Model for the Thermal Conductivity of Plasma-Sprayed Ceramic Coatings, Thin Solid Films, 1984, 112, pp. 89-95.

[8] C.J. Li and A. Ohmori, Relationships between the microstructure and properties of thermally sprayed deposits, J. Therm. Spray Technol., 2002, 11(3), pp. 365-374.

[9] S. Boire-Lavigne, C. Moreau, and R.G. Saint-Jacques, The Relationship between the Microstructure and Thermal- Diffusivity of Plasma-Sprayed Tungsten Coatings, J. Therm. Spray Technol., 1995, 4(3), pp. 261-267.

[10] T.J. Lu, C.G. Levi, H.N.G. Wadley, and A.G. Evans, Distributed porosity as a control parameter for oxide thermal barriers made by physical vapor deposition, J. Am. Ceram. Soc., 2001, 84(12), pp. 2937-2946.

[11] T.J. Lu and J.W. Hutchinson, Thermal-Conductivity and Expansion of Cross-Ply Composites with Matrix Cracks, J. Mech. Phys. Solids, 1995, 43(8), pp. 1175-1198.

[12] D.Y. Tzou, The Effect of Internal Heat-Transfer in Cavities on the Overall Thermal-Conductivity, Int. J. Heat Mass Transf., 1991, 34(7), pp. 1839-1846.

[13] Z. Hashin, The Differential Scheme and Its Application to Cracked Materials, J. Mech. Phys. Solids, 1988, 36(6), pp. 719-734.

[14] T.H. Bauer, A General Analytical Approach toward the Thermal Conductivity of Porous Media, Int. J. Heat Mass Transf., 1993, 36(17), pp. 4181-4191.

[15] I.O. Golosnoy, S.A. Tsipas, and T.W. Clyne, An Analytical Model for Simulation of Heat Flow in Plasma Sprayed Thermal Barrier Coatings, J. Therm. Spray Technol., 2005, 14(2), pp. 205-214.

[16] D.M. Zhu and R.A. Miller, Thermal Conductivity and Elastic Modulus Evolution of Thermal Barrier Coatings under High Heat Flux Conditions, J. Therm. Spray Technol., 2000, 9, pp. 175-180.

[17] A.F. Renteria and B. Saruhan, Effect of ageing on microstructure changes in EB-PVD manufactured standard PYSZ top coat of thermal barrier coatings, J. Eur. Ceram. Soc., 2006, 26, pp. 2249-2255.

[18] M.N. Rahaman, J.R. Gross, R.E. Dutton, and H. Wang, Phase stability, sintering, and thermal conductivity of plasma-sprayed ZrO2-Gd2O3 compositions for potential thermal barrier coating applications, Acta Mater., 2006, 54(6), pp. 1615-1621.

[19] J.A. Thompson and T.W. Clyne, The Effect of Heat Treatment on the Stiffness of Zirconia Top Coats in Plasma-Sprayed TBCs, Acta Mater., 2001, 49(9), pp. 1565-1575.

[20] M. Ahrens, S. Lampenscherf, R. Vassen, and D. Stover, Sintering and creep processes in plasma-sprayed thermal barrier coatings, J. Therm. Spray Technol., 2004, 13(3), pp. 432-442.

[21] S.R. Choi, D.M. Zhu, and R.A. Miller, Effect of sintering on mechanical properties of plasma-sprayed zirconia-based thermal barrier coatings, J. Am. Ceram. Soc., 2005, 88(10), pp. 2859-2867.
[22] L. Singheiser, R. Steinbrech, W.J. Quadakkers, and R. Herzog, Failure aspects of thermal barrier coatings, Mater. High Temp., 2001, 18(4), pp. 249-259.
[23] R. Vassen, N. Czech, W. Mallener, W. Stamm, and D. Stoever, Influence of Impurity Content and Porosity of Plasma-Sprayed Yttria-Stabilized Zirconia Layers on the Sintering Behaviour, Surf. Coat. Technol., 2001, 141, pp. 135-140.
[24] N.M. Yanar, M.J. Stiger, M. Maris-Sida, F.S. Pettit, and G.H. Meier, "The effects of high temperature exposure on the durability of thermal barrier coatings, Key Eng. Mater., 2001, 197, pp. 145-163.
[25] V. Lughi, V.K. Tolpygo, and D.R. Clarke, Microstructural aspects of the sintering of thermal barrier coatings, Mater. Sci. Eng. A, 2004, 272, pp. 215-221.
[26] S.A. Tsipas, I.O. Golosnoy, R. Damani, and T.W. Clyne, The Effect of a High Thermal Gradient on Sintering and Stiffening in the Top Coat of a Thermal Barrier Coating (TBC) System, J. Therm. Spray Technol., 2004, 13(3), pp. 370-376.
[27] S. Kramer, J. Yang, C.G. Levi, and C.A. Johnson, Thermochemical interaction of thermal barrier coatings with molten CaO-MgO-Al2O3-SiO2 (CMAS) deposits, J. Am. Ceram. Soc., 2006, 89, pp. 3167-3175.
[28] X. Chen, Calcium–magnesium–alumina–silicate (CMAS) delamination mechanisms in EB-PVD thermal barrier coatings, Surf. Coat. Technol., 2006, 200, pp. 3418-3427.
[29] T. Strangman, D. Raybould, A. Jameel, and W. Baker, Damage mechanisms, life prediction, and development of EB-PVD thermal barrier coatings for turbine airfoils, Surf. Coat. Technol., 2007, 202, pp. 658-664.
[30] K.M. Grant, S. Kramer, J.P.A.v.d. Lof, and C.G. Levi, CMAS degradation of environmental barrier coatings, Surf. Coat. Technol., 2007, 202, pp. 653-657.
[31] S. Paul, A. Cipitria, I.O. Golosnoy, and T.W. Clyne, Effects of Impurity Content on the Sintering Characteristics of Plasma Sprayed Zirconia, J. Therm. Spray Technol., 2007, 16(5-6), pp. 798-803.
[32] R. Siegel and J.R. Howell, Thermal Radiation Heat Transfer, 1st ed. New York: McGraw-Hill, 1972.
[33] R. Berman, Thermal Conduction in Solids, Oxford: Clarendon, 1976.
[34] P.G. Klemens and R.K. Williams, Thermal Conductivity of Metals and Alloys, Int. Met. Rev., 1986, 31, pp. 197-215.
[35] L.B. Loeb, The Kinetic Theory of Gases, New York: McGraw-Hill, 1934.
[36] T.J. Lu, H.A. Stone, and M.F. Ashby, Heat Transfer in Open-Cell Metal Foams, Acta Mater., 1998, 46(10), pp. 3619-3635.
[37] T.J. Lu, Heat Transfer Efficiency of Metal Honeycombs, Int. J. Heat Mass Transf., 1999, 42, pp. 2031-2040.
[38] C.Y. Zhao, T. Kim, T.J. Lu, and H.P. Hodson, Thermal Transport in High Porosity Cellular Metal Foams, J. Thermophys. Heat Transf., 2004, 18(3), pp. 309-317.
[39] S. Ahmaniemi, P. Vuoristo, T. Mantyla, F. Cernuschi, and L. Lorenzoni, Modified Thick Thermal Barrier Coatings: Thermophysical Characterization, J. Eur. Ceram. Soc., 2004, 24, pp. 2669-2679.
[40] H. Guo, H. Murakami, and S. Kuroda, Thermal cycling behavior of plasma sprayed segmented thermal barrier coatings, Mater. Trans., 2006, 4, pp. 306-309.
[41] H. Hatta and M. Taya, Thermal Conductivity of Coated Filler Composites, J. Appl. Phys., 1986, 59, pp. 1851-1860.
[42] Y. Benveniste and T. Miloh, On the Effective Thermal Conductivity of Coated Short-Fiber Composites, J. Appl. Phys., 1991, 69(3), pp. 1337-1344.
[43] I. Sevostianov, M. Kachanov, J. Ruud, P. Lorraine, and M. Dubois, Quantitative characterization of microstructures of plasma-sprayed coatings and their conductive and elastic properties, Mater. Sci. Eng. A, 2004, 386, pp. 164–174.
[44] I. Sevostianov, L. Gorbatikh, and M. Kachanov, Recovery of information on the microstructure of porous/microcracked materials from the effective elastic/conductive properties, Mater. Sci. Eng. A, 2001, 318(1-2), pp. 1-14.

[45] D. Zhu, N.P. Bansal, K.N. Lee, and R.A. Miller, Thermal Conductivity of Ceramic Thermal Barrier and Environmental Barrier Coating Materials, in NASA TM-2001-211122. 2001, NASA Lewis Research Center: Cleveland, Ohio.

[46] S. Raghavan, H. Wang, R.B. Dinwiddie, W.D. Porter, and M.J. Mayo, The Effect of Grain Size, Porosity and Yttria Content on the Thermal Conductivity of Nanocrystalline Zirconia, Scr. Mater., 1998, 39(8), pp. 1119-1125.

[47] R. Mevrel, J.-C. Laizet, A. Azzopardi, B. Leclercq, M. Poulain, O. Lavigne, and D. Demange, Thermal diffusivity and conductivity of $Zr_{1-x}Y_xO_{2-x/2}$ (x=0, 0.084 and 0.179) single crystals, J. Eur. Ceram. Soc., 2004, 24, pp. 3081–3089.

[48] R. McPherson, A Review of Microstructure and Properties of Plasma Sprayed Ceramics Coatings, Surf. Coat. Technol., 1989, 39/40, pp. 173-181.

[49] P. Bengtsson and T. Johannesson, Characterization of Microstructural Defects in Plasma-Sprayed Thermal Barrier Coatings, J. Therm. Spray Technol., 1995, 4(3), pp. 245-251.

[50] J. Ilavsky, A.J. Allen, G.G. Long, S. Krueger, C.C. Berndt, and H. Herman, Influence of Spray Angle on the Pore and Crack Microstructure of Plasma Sprayed Deposits, J. Am. Ceram. Soc., 1997, 80(3), pp. 733-742.

[51] A.J. Allen, J. Ilavsky, G.G. Long, J.S. Wallace, C.C. Berndt, and H. Herman, Microstructural Characterisation of Yttria-stabilised Zirconia Plasma-sprayed Deposits using Multiple Small-Angle Neutron Scattering, Acta Mater., 2001, 49, pp. 1661-1675.

[52] A. Kulkarni, Z. Wang, T. Nakamura, S. Sampath, A. Goland, H. Herman, J. Allen, J. Ilavsky, G. Long, J. Frahm, and R.W. Steinbrech, Comprehensive microstructural characterization and predictive property modeling of plasma-sprayed zirconia coatings, Acta Mater., 2003, 51(9), pp. 2457-2475.

[53] H. Boukari, A.J. Allen, G.G. Long, J. Ilavsky, J.S. Wallace, C.C. Berndt, and H. Herman, Small-angle neutron scattering study of the role of feedstock particle size on the microstructural behavior of plasma-sprayed yttria-stabilized zirconia deposits, J. Mater. Res., 2003, 18(3), pp. 624-634.

[54] S. Paul, I.O. Golosnoy, A. Cipitria, T.W. Clyne, L. Xie, and M.R. Dorfman, "Effect of Heat Treatment on Pore Architecture and Associated Property Changes in Plasma Sprayed TBCs" in International Thermal Spray Conference CD, 2007, Beijing, China: ASM International, Materials Park, Ohio, USA.

[55] D.M. Zhu and R.A. Miller, Sintering and Creep Behaviour of Plasma-Sprayed Zirconia- and Hafnia-Based Thermal Barrier Coatings, Surf. Coat. Technol., 1998, 109(1-3), pp. 114-120.

[56] R.W. Trice, Y.J. Su, J.R. Mawdsley, K.T. Faber, A.R. De Arellano-Lopez, H. Wang, and W.D. Porter, Effect of Heat Treatment on Phase Stability, Microstructure, and Thermal Conductivity of Plasma-sprayed YSZ, J. Mater. Sci., 2002, 37(11), pp. 2359-2365.

[57] R. Siegel and C.M. Spuckler, Analysis of Thermal Radiation Effects on Temperatures in Turbine Engine Thermal Barrier Coatings, Mater. Sci. Eng. A, 1998, 245(2), pp. 150-159.

[58] V.A. Petrov and A.P. Chernyshev, Thermal-radiation Properties of Zirconia when heated by Laser Radiation up to the Temperature of High-rate Vaporization, High Temperature, 1999, 37(1), pp. 58-66.

[59] J.I. Eldridge, C.M. Spuckler, K.W. Street, and J.R. Markham, Infrared Radiative Properties of Yttria-Stabilized Zirconia Thermal Barrier Coatings, Ceram. Eng. Sci. Proc., 2002, 23(4), pp. 417-430..

[60] E. Litovsky, M. Shapiro, and A. Shavit, Gas pressure and temperature dependences of thermal conductivity of porous ceramic materials. 2. Refractories and ceramics with porosity exceeding 30%, J. Am. Ceram. Soc., 1996, 79(5), pp. 1366-1376.

[61] CRC, Handbook of Chemistry and Physics, 57th ed, R.C. Weast, Ed., Cleveland: CRC Press, 1976.

[62] T.J. Lu, C.G. Levi, H.N.G. Wadley, and A.G. Evans, Distributed Porosity as a Control Parameter for Oxide Thermal Barriers made by Physical Vapor Deposition, J. Am. Ceram. Soc., 2001, 84, pp. 2937-2946.

[63] G. Kaye and T. Laby, Tables of Physical and Chemical Constants, 14th ed., London: Longman, 1973.

[64] F.P. Incropera and D.P. Dewitt, Introduction to Heat Transfer*,* 3rd ed., NY, USA: John Wiley & Sons, Inc., 1996.

[65] A.C. Fox and T.W. Clyne, The Gas Permeability of Plasma Sprayed Ceramic Coatings, in Thermal Spray: A United Forum for Scientific and Technological Advances. Proceedings of the 1st United Thermal Spray Conference, C.C. Berndt, Ed., 1998, ASM: Indianapolis, USA. p. 483-490.
[66] A.C. Fox and T.W. Clyne, Oxygen Transport through the Zirconia Layer in Plasma Sprayed Thermal Barrier Coatings, Surf. Coat. Technol., 2004, 184, pp. 311-321.
[67] M. Öziçik, Heat Conduction, New York: John Wiley & Sons, 1979.
[68] T. Makino, T. Kunitomo, I. Sakai, and H. Kinoshita, Thermal Radiation Properties of Ceramic Materials, Heat Transfer. Japanese Research, 1984, 13(4), pp. 33-50.
[69] F.A. Akopov, G.E. Val'yano, A.Y. Vorob'ev, V.N. Mineev, V.A. Petrov, A.P. Chernyshev, and G.P. Chernyshev, Thermal radiative properties of ceramic of cubic ZrO2 stabilized with Y2O3 at high temperatures, High Temperature, 2001, 39(2), pp. 244-254.
[70] F. Cabannes and D. Billard, Measurement of Infrared-Absorption of Some Oxides in Connection with the Radiative-Transfer in Porous and Fibrous Materials, Int. J. Thermophys., 1987, 8(1), pp. 97-118.
[71] A. Ferriere, L. Lestrade, and J.F. Robert, Optical properties of plasma-sprayed ZrO2-Y2O3 at high temperature for solar applications, J. Sol. Energy Eng. (Trans. ASME), 2000, 122(1), pp. 9-13.
[72] D.R. Clarke, Materials Selection Guidelines for Low Thermal Conductivity Barrier Coatings, Surf. Coat. Technol., 2003, 163-164, pp. 67-74.
[73] H.J. Ratzer-Scheibe, U. Schulz, and T. Krell, The effect of coating thickness on the thermal conductivity of EB-PVD PYSZ thermal barrier coatings, Surf. Coat. Technol., 2006, 200(18-19), pp. 5636-5644.
[74] H.J. Ratzer-Scheibe and U. Schulz, The effects of heat treatment and gas atmosphere on the thermal conductivity of APS and EB-PVD PYSZ thermal barrier coatings, Surf. Coat. Technol., 2007, 201, pp. 7880-7888.
[75] L. Xie, M.R. Dorfman, A. Cipitria, S. Paul, I.O. Golosnoy, and T.W. Clyne, Properties and Performance of High Purity Thermal Barrier Coatings, J. Therm. Spray Technol, 2007, 16(5-6), pp. 804-808.
[76] A. Cipitria, I.O. Golosnoy, and T.W. Clyne, Sintering Kinetics of Plasma-Sprayed Zirconia TBCs, J. Therm. Spray Technol., 2007, 16(5-6), pp. 809-815.
[77] A. Cipitria, I.O. Golosnoy, and T.W. Clyne, A Sintering Model for Plasma-Sprayed Zirconia TBCs. Part I: Free-Standing Coatings, Acta Mater., 2009, 57, pp. 980–992.
[78] S. Paul, A. Cipitria, S.A. Tsipas, and T.W. Clyne, Sintering Characteristics of Plasma Sprayed Zirconia Coatings containing different Stabilisers, Surf. Coat. Technol., 2009, 203, pp. 1069-1074.
[79] H.E. Eaton and R.C. Novak, Sintering Studies of Plasma Sprayed Zirconia, Surf. Coat. Technol., 1987, 32, pp. 227-236.
[80] S. Siebert, C. Funke, R. Vassen, and D. Stover, Changes in Porosity and Young's Modulus due to Sintering of Plasma-Sprayed Thermal Barrier Coatings, J. Mater. Process. Technol., 1999, 93, pp. 217-223.
[81] J. Pan, A.C.F. Cocks, and S. Kucherenko, Finite Element Formulation of Coupled Grain-Boundary and Surface Diffusion with Grain-Boundary Migration, Proc. Roy. Soc. Lond. A: Math. Phys. Sci., 1997, 453, pp. 2161-2184.
[82] A.C.F. Cocks, S.P.A. Gill, and J. Pan, Modeling Microstructure Evolution in Engineering Materials, Advances in Applied Mechanics, 1999, 36, pp. 81-162.
[83] J. Pan, Modelling Sintering at Different Length Scales, Int. Mater. Rev., 2003, 48(2), pp. 69-85.
[84] R.G. Hutchinson, N.A. Fleck, and A.C.F. Cocks, A Sintering Model for Thermal Barrier Coatings, Acta Mater., 2006, 54(5), pp. 1297-1306.
[85] A. Cipitria, I.O. Golosnoy, and T.W. Clyne, A Sintering Model for Plasma-Sprayed Zirconia TBCs. Part II: Coatings bonded to a Rigid Substrate, Acta Mater., 2009, 57, pp. 993–1003.
[86] J.C. Tan, S.A. Tsipas, I.O. Golosnoy, S. Paul, J.A. Curran, and T.W. Clyne, A Steady-State Bi-Substrate Technique for Measurement of the Thermal Conductivity of Ceramic Coatings, Surf. Coat. Technol., 2006, 201(3-4), pp. 1414-1420.

[87] S.E. Gustafsson, Transient Plane Source Techniques for Thermal Conductivity and Thermal Diffusivity Measurements of Solid Materials, Review of Scientific Instruments, 1990, 62(3), pp. 797-804.

[88] S. Paul, "Pore Architecture in Ceramic Thermal Barrier Coatings, in Materials Science & Metallurgy", PhD thesis, University of Cambridge: Cambridge, 2007.

[89] R. Vassen, R. Traeger, and D. Stover, Correlation Between Spraying Conditions and Microcrack Density and their Influence on Thermal Cycling Life of Thermal Barrier Coatings, J. Therm. Spray Technol., 2004,13(3), pp. 396-404.

[90] A. Kulkarni, J. Gutleber, S. Sampath, A. Goland, W.B. Lindquist, H. Herman, A.J. Allen, and B. Dowd, Studies of the microstructure and properties of dense ceramic coatings produced by high-velocity oxygen-fuel combustion spraying, Mater. Sci. Eng. A, 2004, 369(1-2), pp. 124-137.